



Optics Letters

Enhanced total internal reflection using low-index nanolattice materials

XU A. ZHANG, YI-AN CHEN, ABHIJEET BAGAL, AND CHIH-HAO CHANG* 

Department of Mechanical and Aerospace Engineering, North Carolina State University, Raleigh, North Carolina 27695, USA

*Corresponding author: chichang@ncsu.edu

Received 4 August 2017; revised 14 September 2017; accepted 16 September 2017; posted 19 September 2017 (Doc. ID 303972); published 9 October 2017

Low-index materials are key components in integrated photonics and can enhance index contrast and improve performance. Such materials can be constructed from porous materials, which generally lack mechanical strength and are difficult to integrate. Here we demonstrate enhanced total internal reflection (TIR) induced by integrating robust nanolattice materials with periodic architectures between high-index media. The transmission measurement from the multilayer stack illustrates a cutoff at about a 60° incidence angle, indicating an enhanced light trapping effect through TIR. Light propagation in the nanolattice material is simulated using rigorous coupled-wave analysis and transfer matrix methods, which agrees well with experimental data. The demonstration of the TIR effect in this Letter serves as a first step towards the realization of multilayer devices with nanolattice materials as robust low-index components. These nanolattice materials can find applications in integrated photonics, antireflection coatings, photonic crystals, and low- k dielectric. © 2017 Optical Society of America

OCIS codes: (160.4670) Optical materials; (160.4236) Nanomaterials; (260.6970) Total internal reflection; (310.6628) Subwavelength structures, nanostructures; (310.6860) Thin films, optical properties.

<https://doi.org/10.1364/OL.42.004123>

The material refractive index is the key factor in determining the performance of photonic structures and devices. It is often desirable to have large index contrasts in order to enhance light-matter interactions in photonic structures, such as photonic crystals [1], distributed Bragg reflectors [2], low-loss waveguides [3], and high- Q cavities [4]. Total internal reflection (TIR), a well-known optical phenomenon that occurs when light travels from a high-index to a low-index medium, can also benefit. Governed by the index contrast between the two media, the TIR critical angle can be decreased to enhance light trapping when a low-index material is used. While air is most often used as the low-index medium with $n_{\text{air}} = 1$, it is difficult to implement in integrated optical devices consisting of multiple layers. In these cases, a physical layer with a low refractive index is necessary for mechanical support.

Although naturally occurring materials with low refractive indices are limited, there are significant research efforts to artificially create low-index materials close to the index of air. These new materials consist of porous structures through various conventional fabrication techniques, such as oblique deposition [5–9], the sol-gel process [10], and chemical vapor deposition [11]. Due to the air voids, the fabricated porous structures can have effective refractive indices lower than the solid material components. However, such materials typically lack mechanical stability and can induce optical scattering because of the random architectures of the structures. As a result, integrating these porous materials into photonic structures can pose challenges, such as potential structural collapsing and degradation of low-index properties. Our recent work demonstrated a new class of nanolattice materials with periodic architectures using a combination of three-dimensional (3D) nanolithography and atomic layer deposition (ALD) [12]. By controlling the shell thickness, lattice geometry, and material composition, the refractive index of these nanolattices can be designed to be between 1 and 1.3. Compared with random architectures, periodic architectures offer advantages in designing the refractive index, enhancing mechanical stability, and reducing optical scattering. It is also important to note that the nanolattice materials with periodic architectures only need half the amount of materials to show similar mechanical properties, compared with aerogel-like materials consisting of random architectures, as shown in our previous work [12]. With these attractive properties, the nanolattice materials can potentially be suitable materials in integrated multilayer photonic structures. However, in the previous work, the low index was characterized using macroscopic approaches with spectroscopic ellipsometry, and it is not clear how light would propagate in such nanolattice materials.

Here we demonstrate the enhancement of the TIR effect from a multilayer consisting of the low-index nanolattice materials integrated between two high-index media. The transmission of the fabricated sample is characterized experimentally and exhibits a rapid decrease at around 50° incident angle, an indication of critical angle, and the TIR effect. The multilayer system is modeled in rigorous coupled-wave analysis (RCWA) and the transfer-matrix (T-matrix) method and agrees with experimental data. The optical images of the nanolattice

materials above the critical angle show a clear image from reflection and none from transmission, which serves as a demonstration of the TIR effect. These results not only confirm the low-index behavior of the nanolattice materials, but also enable their integration into multilayer structures to enhance light trapping for photonic applications.

The TIR effect is a well-known effect that occurs when light passes from a high-index to a low-index medium. The system to be studied is shown in Fig. 1(a), where the nanolattice material on a glass substrate is sandwiched between two polydimethylsiloxane (PDMS) half-spheres. When the incident angle θ is larger than the critical angle θ_c , the reflection can reach 100%, and no transmitted light is present. Note that if the nanolattice material has an index higher than PDMS, no TIR would be observed. In this Letter, the occurrence of TIR is examined using nanolattice materials made from Al_2O_3 with a 16 nm shell thickness using ALD and 3D nanolithography, as described in our previous work [12]. The nanolattice material being studied is shown in the scanning electron micrograph in Fig. 1(b), and has a total film thickness of 1 μm , a period of 500 nm, porosity of 83.1%, and a measured effective index of 1.10.

To characterize the TIR effect of the nanolattice materials, two identical PDMS half-spheres are bonded to either side of the sample. The mixing ratio of PDMS was 10:1 for the base and crosslinker. The holes on the nanolattice materials were capped with a thin PDMS layer, transferred after 6000 rpm spin-coating on a silicon substrate. Then a UV-curable optical adhesive (NOA61, Norland Optical Adhesive) was applied to the two interfaces between the PDMS half-spheres and the nanolattice material. It was found that fast curing under strong UV light can cause large bubbles in the adhesive, which leads the nanolattice material to collapse. Therefore, slow curing was performed under ambient room condition for 10 h. No bubbles were found after the slow curing of optical adhesives. While only the nanolattice material with a 16 nm shell is tested, the measurement method can be applied to other types of nanolattice materials with different shell thicknesses and materials.

The optical transmission of the prepared sample was then measured using both a 633 nm HeNe laser (Model 30995, Research Electro-Optics, Inc.) and a 532 nm solid-state laser (Model 85-GCB-020, Melles Griot). A rotation stage (RSP-1T, Newport Co.) was used to rotate the sample to change incident angles from 0° to 70° with 1° resolution. For incident angles larger than 70° , the illumination area exceeded the area of the nanolattice material; thus, the angles are not considered.

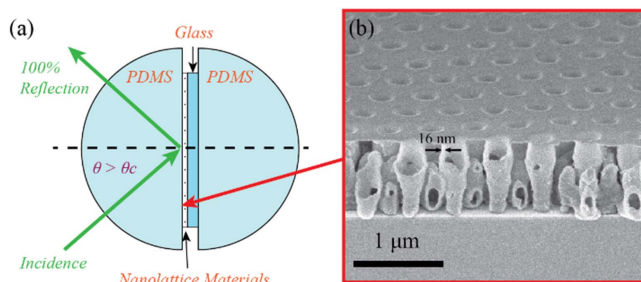


Fig. 1. (a) Schematic for measuring the TIR effect from nanolattice materials sandwiched between two PDMS half-spheres. θ is the incident angle, while θ_c is the critical angle. (b) Scanning electron microscope image of the nanolattice materials under study. The nanolattice material is made from Al_2O_3 with a 16 nm shell thickness.

A photodiode detector (Model 918D-UV-OD3, Newport Co.) was used to measure the transmitted light intensity. The transmission for both transverse electric (TE) and transverse magnetic (TM) polarizations was characterized.

The multilayer stack consisting of the nanolattice material, as shown in Fig. 1(a), was modeled using RCWA [13,14]. The RCWA model was based on a hollow rectangle Al_2O_3 ($n = 1.63$) column periodic along both x and y directions. The lattice is approximated as a square lattice with a 500 nm period and 16 nm thick Al_2O_3 shells. The model was constructed so that the resulting effective refractive index based on the calculations from the Maxwell–Garnett effective medium theory [15–17] is approximately equal to that of the fabricated nanolattice material. The top and bottom layer materials are PDMS ($n = 1.40$) and glass ($n = 1.50$), respectively, and modeled as semi-infinite media. In addition, a T-matrix method was also used to simulate the structure. The T-matrix method calculates light transmission in multilayered structures using a matrix formulation of wave equations and applying boundary conditions at each interface. The nanolattice material is approximated as a homogeneous film with a uniform refractive index ($n = 1.13$) in the T-matrix, while the internal structures of the nanolattice materials are taken into account in RCWA. Note that possible collapsing of nanolattice materials can occur during the curing of optical adhesive. As no direct way was found to measure the degree of collapse, calculations revealed that a roughly 30% collapse in terms of structure height was a reasonable estimate to achieve good fitting between experiments and simulations. In accordance with the estimated collapse, a higher refractive index ($n = 1.13$) was used in the T-matrix modeling, compared with the lower index ($n = 1.10$) before integration of nanolattice materials.

The transmission measurement and theoretical calculation results for 532 nm and 633 nm wavelengths and both TE and TM polarization states are plotted in Fig. 2. The experimental data were corrected using Fresnel equations to account for reflection losses at the adhesion layers. The reflection losses are small due to a low-index mismatch, and account for 0.1%–1.3% in the 0° – 70° angle range, respectively. This offers a direct comparison to theoretical models that were based on the three-layer approximation. The inset in Fig. 2(a) illustrates the simplified model consisting of hollow rectangular tubes used in RCWA. For experimental results, rapid transmission decrease can be observed for all four cases starting from around a 40° incident angle. These results agree with the critical angle of 53.8° calculated from the PDMS and nanolattice indices of 1.40 and 1.13, respectively. Note that the theoretical models show transmission decrease at larger angles near 50° . Despite this disagreement, at roughly 60° incidence, both experimentally measured and theoretically calculated transmission curves approach zero, indicating TIR. The TIR effect is confirmed by the RCWA and the T-matrix, also plotted in Fig. 2 as red and blue lines, respectively. These results demonstrate that TIR can be enhanced by using low-index nanolattice material.

While the experimental data follow the trends predicted by the T-matrix and RCWA, there are mismatches in some areas. The experimental measurements indicate a more gradual, continuous decrease in transmission. This can be attributed to the thickness of the low-index layer, which is similar to the operating wavelength and can lead to the coupling of evanescent waves. Thicker low-index films are thus preferred to achieve

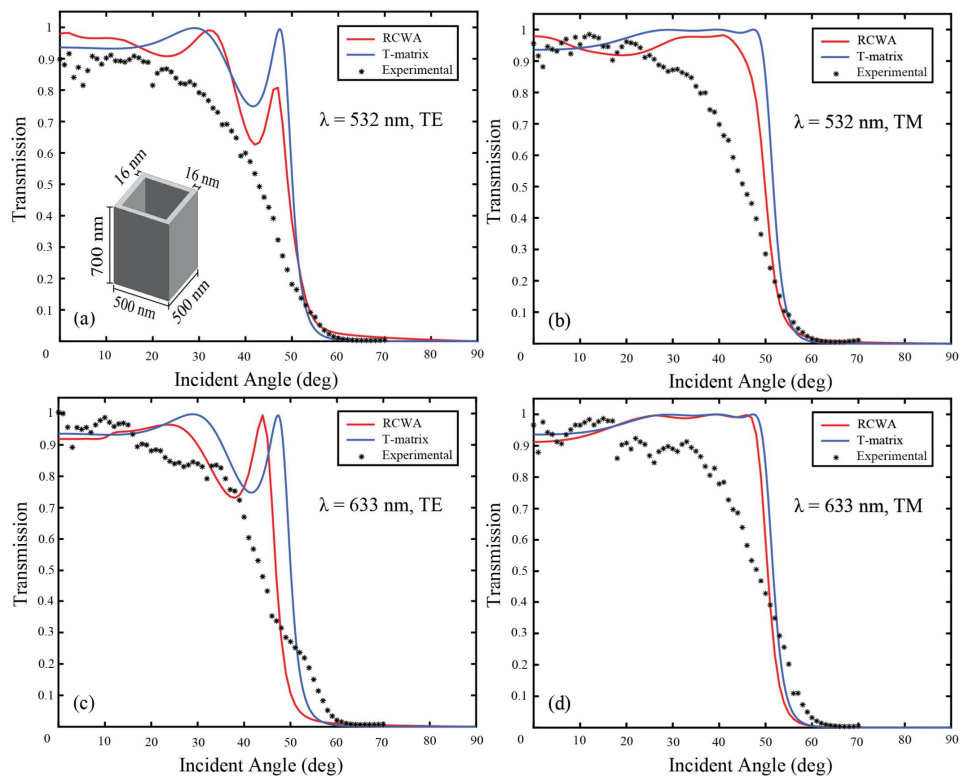


Fig. 2. Angular transmission results from experimental measurements, compared with RCWA and T-matrix modeling for (a) a 532 nm wavelength in TE polarization, (b) a 532 nm wavelength in TM polarization, (c) a 633 nm wavelength in TE polarization, and (d) a 633 nm wavelength in TM polarization. The inset in (a) shows the rectangular tube models for RCWA calculations.

TIR. The modeling results also show intensity oscillation due to thin-film interference effects, and thicknesses and refractive indices of each layer can influence the critical angle and local transmission maximum/minimum. The TE and TM data also display similarities, which is unexpected given the Brewster angle effect shown in the model. This can be attributed to the 3D nature of the nanolattice material, which is not included in the two-dimensional tubular RCWA approximation. The trend mismatches can also be due to the scattering in PDMS, the

imperfect shapes of the PDMS half-spheres, and partial and/or non-uniform collapse of nanolattice material structure. However, the existence of these mismatches does not prevent demonstration of the enhanced TIR effect at the predicted critical angle, which is the main focus of this Letter. The role of 3D lattice geometry on TE and TM polarized light will be studied further in future work.

The TIR effect of nanolattice materials can also be visually observed, as illustrated in Fig. 3. Here pictures of nanolattice

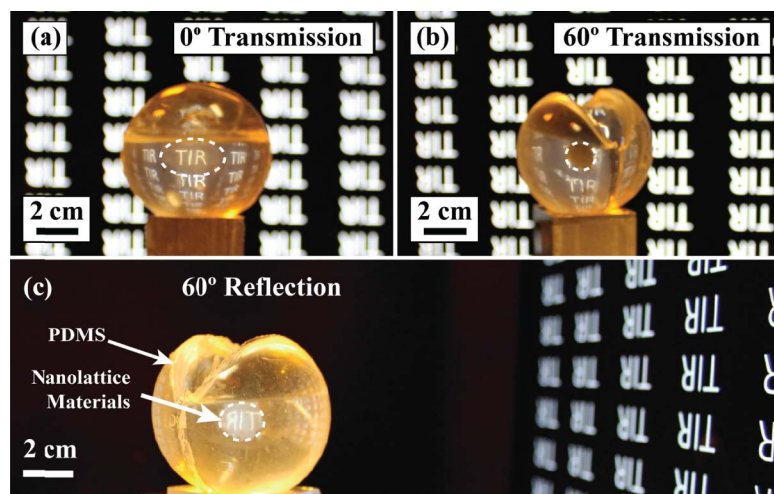


Fig. 3. Reflection and transmission of nanolattice materials from a computer screen. (a) Clear image is shown at 0° transmission through nanolattice materials. (b) Screen image is not present at 60° transmission through nanolattice materials. (c) 60° reflected image from a computer screen. The dashed lines in each panel show the approximate boundaries of the nanolattice material.

materials at 0° and 60° incident angles were taken to observe the reflected and transmitted images from a computer screen (the video of the experiment can be seen in [Visualization 1](#)). Due to the image inversion effect of the PDMS ball lens, the image on the computer screen is rotated 180° . For normal incidence at a 0° angle, the virtual image of upright “TIR” letters can be observed in transmission for both the areas with and without nanolattice materials, as shown in Fig. 3(a). Here the nanomaterial does not alter the image since the incident angle is below the TIR critical angle. At a 60° incident angle, however, the image cannot be observed in transmission for the area with nanolattice material to indicate TIR, as shown in Fig. 3(b). Note that in the area without the nanolattice materials, the letters on the computer display can be observed in transmission since there is no TIR. At the same incident angle, a clear mirror image of “TIR” can be observed in reflection for the area with nanolattice material, as shown in Fig. 3(c). Note that the mirror image can only be observed in the nanolattice material area where TIR occurs, and not in the other areas. These results demonstrate the existence of the enhanced TIR effect using the integrated nanolattice materials. The virtual images formed from reflection and transmission in the area of nanolattice materials are clear, indicating low optical scattering. This is one of the major advantages of nanolattice materials with periodic architectures, and can be applied in integrated photonic devices with low losses.

A potential challenge for integration lies in the fact that the top surface of nanolattice materials is also porous so that direct deposition of other photonic layers is difficult. One work used direct deposition of a thin layer on the porous structure to cover the top surface in order to apply the next photonic structures [5]. However, it requires that the pores on top surface are small enough to prevent the deposited materials from filling the entire structures. Since the nanolattice materials in this Letter have relatively large pores (~ 200 nm in diameter) on top surface, direct deposition of materials can potentially fill the entire structures. Therefore, a thin PDMS cover layer was used to seal the porous top surface to glue the PDMS half-sphere. Other nanofabrication methods are also currently being investigated to directly create a continuous flat top surface during nanolattice materials fabrication to eliminate cover layers when integrating with other photonic structures. In addition, more studies on the nanolattice will be conducted in terms of material type, porous geometry, height, and scalable manufacturing. These studies will open more possibilities of even lower refractive indices with robust mechanical properties, and new optical phenomena, such as frustrated TIR.

In conclusion, we have demonstrated an enhanced TIR effect using nanolattice low-index materials. The nanolattice materials consist of periodic architectures, which serve as a strong mechanical support while possessing a refractive index close to air. Its enhanced mechanical strength allows the integration into multilayer photonic systems, as demonstrated by the successful incorporation of nanolattice materials between PDMS

half-spheres. The transmission of the nanolattice materials shows zero transmission at around 60° , confirming the enhanced TIR effect. The measurement and modeling methods developed in this Letter can be readily applied to other nanolattice materials with varied material and geometry types. The demonstration of the enhanced TIR effect is a first step to show the possibility of integrating nanolattice materials into multilayer photonic systems, and paves the way for many potential photonic applications using this new class of low-index materials.

Funding. National Science Foundation (NSF) Faculty Early Career Development (CAREER) Program (CMMI#1552424).

Acknowledgment. The authors are grateful to the NCSU Nanofabrication Facility (NNF) and Analytical Instrumentation Facility (AIF) at North Carolina State University, supported by the State of North Carolina and the NSF. The NNF and AIF are members of the North Carolina Research Triangle Nanotechnology Network (RTNN), a site in the National Nanotechnology Coordinated Infrastructure (NNCI).

REFERENCES

1. B. Temelkuran, S. D. Hart, G. Benoit, J. D. Joannopoulos, and Y. Fink, *Nature* **420**, 650 (2002).
2. S.-T. Ho, S. L. McCall, R. E. Slusher, L. N. Pfeiffer, K. W. West, A. F. J. Levi, G. E. Blonder, and J. L. Jewell, *Appl. Phys. Lett.* **57**, 1387 (1990).
3. M. Schmidt, G. Boettger, M. Eich, W. Morgenroth, U. Huebner, R. Boucher, H. G. Meyer, D. Konjhodzic, H. Bretinger, and F. Marlow, *Appl. Phys. Lett.* **85**, 16 (2004).
4. L. Wang, S.-X. Zhang, Q. Song, Q. Gong, and Y.-F. Xiao, *Optica* **3**, 937 (2016).
5. J.-Q. Xi, M. F. Schubert, J. K. Kim, E. F. Schubert, M. Chen, S.-Y. Lin, W. Liu, and J. A. Smart, *Nat. Photonics* **1**, 176 (2007).
6. J.-Q. Xi, J. K. Kim, and E. F. Schubert, *Nano Lett.* **5**, 1385 (2005).
7. J.-Q. Xi, J. K. Kim, E. F. Schubert, D. Ye, T.-M. Lu, S.-Y. Lin, and J. S. Juneja, *Opt. Lett.* **31**, 601 (2006).
8. Z. Wang, P. R. West, X. Meng, N. Kinsey, V. M. Shalae, and A. Boltasseva, *MRS Commun.* **6**, 17 (2016).
9. U. Guler, D. Zemlyanov, J. Kim, Z. Wang, R. Chandrasekar, X. Meng, E. Stach, A. V. Kildishev, V. M. Shalae, and A. Boltasseva, *Adv. Opt. Mater.* **5**, 1600717 (2017).
10. N. Kawakami, Y. Fukumoto, T. Kinoshita, K. Suzuki, and K. Inoue, *Jpn. J. Appl. Phys.* **39**, L182 (2000).
11. Z.-P. Yang, L. Ci, J. A. Bur, S.-Y. Lin, and P. M. Ajayan, *Nano Lett.* **8**, 446 (2008).
12. X. A. Zhang, A. Bagal, E. C. Dandley, J. Zhao, C. J. Oldham, B.-I. Wu, G. N. Parsons, and C.-H. Chang, *Adv. Funct. Mater.* **25**, 6644 (2015).
13. M. G. Moharam, T. K. Gaylord, E. B. Grann, and D. A. Pommet, *J. Opt. Soc. Am. A* **12**, 1068 (1995).
14. M. G. Moharam and T. K. Gaylord, *J. Opt. Soc. Am.* **71**, 811 (1981).
15. J. C. M. Garnett, *Philos. Trans. R. Soc. London* **203**, 385 (1904).
16. N. J. Hutchinson, T. Coquil, A. Navid, and L. Pilon, *Thin Solid Films* **518**, 2141 (2010).
17. P. Sarafis and A. G. Nassiopoulou, *Nano. Res. Lett.* **9**, 418 (2014).